

Electrodeposition and Characterization of W-rich NiW Alloys from Citrate Electrolyte

Mohamed Benaicha^{1,*}, Mahdi Allam², Achour Dakhouché², Meriem Hamla¹

¹ Energetic and Solid-State Electrochemistry Laboratory, Dept. of Processes Engineering, Faculty of Technology, Ferhat Abbas-Setif1 University, Setif, 19000, Algeria.

² Department of chemistry, Faculty of Sciences, Mohamed Boudiaf University, M'sila, 28000, Algeria.

*E-mail: mdbenaicha@yahoo.fr

Received: 21 May 2016/ Accepted: 11 July 2016 / Published: 7 August 2016

The electrodeposition of NiW alloys from citrate electrolyte was studied in an effort to evaluate the effect of applied potential and solution pH on the composition limit and the properties of the deposits. Electrochemical measurements employing cyclic voltammetry (CV), potentiodynamic polarization and electrochemical impedance spectroscopy (EIS) were used to investigate the codeposition process, corrosion resistance and HER electrocatalytic properties of the deposits. The deposits morphology was characterized by scanning electron microscopy (SEM) and the surface composition of coatings was ascertained by Energy dispersive x-ray analysis (EDXA). Possibility of W-rich NiW alloys electrodeposition from ammonia-free citrate electrolyte at room temperature was confirmed. The tungsten content was close to 32 at.% in deposits obtained from a quasi-neutral solution. Structural study revealed that all of NiW coated alloys were amorphous regardless of W content. On the other hand, it was found that Ni-W alloys deposited at -1.4 V/CSE (having about 14 at.% W) are good electrode materials as cathode for HER following the Volmer-Heyrovsky mechanism with substantial surface-adsorbed hydrogen while alloys plated at -1.2 V/SCE (having about 32 wt.% W) were of excellent corrosion resistance in 3.5% NaCl solution.

Keywords: Nickel-tungsten alloys; Electrodeposition; Hydrogen evolution reaction; Electrocatalysis; Corrosion.

1. INTRODUCTION

With the growing demand for clean fuels and consciousness of environmental issues, hydrogen fuel generated from renewable energy sources is commonly regarded as a viable and environmental friendly solution to the world energy needs in the future [1]. Molecular hydrogen can be generated via water electrolysis to sustain a renewable hydrogen economy. However this technology is still

immature with performance disappointing when compared to natural gas reforming, which is the actually preferred method [2]. Among the technical efforts to make this technique competitive is the development of low cost, stable and efficient electrolysis systems.

The operating cell voltage to produce hydrogen by electrolysis of water is given by:

$$V_{op} = E_{rev} + \eta_a + |\eta_c| + IR$$

Where E_{rev} refers to the reversible thermodynamic decomposition voltage ($\approx 1.23\text{V}$), η_a and η_c the anode and cathode overpotentials, and IR the interelectrode ohmic drop. It is worth noting that while ohmic drop can be reduced by enhancing the bath conductivity and minimization of the space between the electrodes, overpotentials for hydrogen (and oxygen) depend on the electrode materials and are major cause for excessive consumption of electrical energy. This fact motivates the extensive research being conducted for the development of efficient and low-cost catalyst materials. It is well established that the Pt-group metals are the best electrocatalysts for hydrogen evolution as the reaction is essentially thermo-neutral ($\Delta G \approx -0.1\text{ eV}$). The next ideal HER catalysts are Ni and Co ($\Delta G \approx -0.28\text{ eV}$) followed by Mo ($\Delta G \approx -0.36\text{ eV}$) and W ($\Delta G \approx -0.42\text{ eV}$) [3]. Interestingly, alloys made of the combination of these metals could be more active for HER than the elemental metals. Navaro –Flores *et al.* [4] reported that alloying nickel with tungsten, molybdenum or iron could increase the intrinsic electrocatalytic activity for the HER compared to pure nickel. More recently, Elias and co-workers [5] reported that the required potential for the HER is about 0.38 V more positive on Ni-W alloy compared to that on both Ni and W, as individual metals. On the other hand, NiW alloys are known for their excellent technological properties such as hardness, thermal stability, wear resistance [6-7] and corrosion resistances at high temperatures [8-9]. Hence, electrodeposited NiW alloys are considered as promising candidates for the development of advanced and inexpensive electrocatalysts to replace platinum-based materials for the production of hydrogen [5, 10]. According to Brenner's classification [8], the electrocrystallisation process of NiW alloys is an induced codeposition system. Opposite to nickel, tungsten cannot be electrodeposited separately from an aqueous solution of any soluble salt of this element, whereas its codeposition with iron-group metals is possible.

A typical electrolyte for the codeposition of NiW alloys consists of an aqueous solution of NiSO_4 , Na_2WO_4 , and Na_3Cit as complexing agent at an elevated temperature of 70-80 °C [11]. Ammonia is commonly used to improve the current efficiency and fine-tune the pH to the chosen value. On the other hand, it reduces the bath stability owing to its rapid evaporation. Usually, the concentration of tungsten in the electroplated alloys is rather low, in the range of 5-15 at.%. Only few works on the deposition of NiW alloys containing high concentrations of tungsten have been reported. Younes *et al.* [12] claimed that removing ammonia from the plating bath helped to increase the W content of the alloy up to 50 at.%. More recently Hong *et al.* [13] reported the deposition of Ni-W alloys having over 40 at. % W. from an acidic electrolyte containing boric acid and sodium citrate at a fixed potential of -1.6 V vs. SCE. However the electrocatalytic and corrosion resistance properties of such alloys are still not well elucidated.

The present work aims to investigate the electrochemical aspects in the deposition process of tungsten-rich nickel-tungsten alloys from an ammonia-free citrate electrolyte operating at room temperature. Particular attention was paid to the influence of pH and applied potential, consequently

the tungsten content, on the corrosion resistance and electrocatalytic activity of electrodeposited Ni-W films for hydrogen evolution reaction (HER) in alkaline water electrolysis.

2. EXPERIMENTAL

The electrochemical experiments were carried out in a conventional three-electrode setup containing 75 ml solution, employing a Voltalab potentiostat-galvanostat (model PGZ 301) to run cyclic voltammetry and perform electrochemical impedance spectroscopy (EIS) measurements or to deposit the films under potentiostatic regime. All solutions were made from analytical-grade chemicals (Sigma-Aldrich, USA) and doubly distilled water. The electrodeposition of Ni/W alloys was studied in a plating bath containing 0.2M Na_2WO_4 , 0.25M $\text{NiSO}_4 \cdot 6\text{H}_2\text{O}$ and 0.05M $\text{NiCl}_2 \cdot 6\text{H}_2\text{O}$ used as the electro-active species and 0.4M $\text{Na}_3\text{C}_6\text{H}_5\text{O}_7 \cdot 2\text{H}_2\text{O}$ (tri-sodium citrate dihydrate) as a complexing agent to bring closer the deposition potentials of the metals and facilitate their codeposition (standard electrode potentials of Ni and W are nearly 0.3 V apart). No boric acid was added to the electrolyte since citrate ions are environmentally friendly and can function as a complexing [14], buffering [14-15], brightening [16] and levelling agent [17] in nickel and its alloying electrolytes. In addition, citrate electrolyte provided higher W contents than with those based on tartrate or malate [18]. Nickel chloride was added to the plating bath in small amount to increase conductivity and uniformity of coating thickness distribution. Moreover, chlorides tend to refine grain size and minimize formation of nodules and trees [19]. The solution was bubbled with clean nitrogen gas to reduce the influence of oxygen during electrodeposition. The bath temperature was maintained at the desired value with an accuracy of ± 1 °C by thermostat water tank and the pH adjusted by addition of sulfuric acid or sodium hydroxide as needed and monitored precisely with a calibrated pH-meter (WTW- inoLab pH 7310). The test specimens (platinum wire and pure copper sheets sized $1 \times 2 \text{ cm}^2$) were used as working electrodes, a platinum foil of high active surface area as the auxiliary electrode and a saturated calomel electrode (SCE) was used as the reference to which all potentials in this paper are referred (unless noted otherwise). To obtain reproducible results, the working electrode surface was polished to a mirror finish with successive grades of alumina powder (Banner Scientific Co. Ltd.) on a Metron polishing cloth. The samples were then degreased with alcohol and rinsed with distilled water before every experiment.

X-ray diffraction (XRD) patterns were obtained with copper K_α radiation source ($\lambda_{K_\alpha} = 1.5418 \text{ \AA}$) on a powder diffractometer (Philips X'Pert Pro Multipurpose X-ray diffractometer). Surface topography and composition of the deposits were examined using a scanning electron microscope (SEM, JEOL 6301 F) combined with an energy dispersive X-ray spectroscope (EDS, Oxford Link Pentafet Detector -INCA software- coupled with a JEOL 6400 unit) using an acceleration voltage up to 20 kV. The accuracy of the measurements was rated as ± 1 wt%. To investigate the corrosion resistance and catalytic activities of electrocoated NiW films for hydrogen evolution reaction (HER) in a 3.5 % NaCl and 30% KOH solutions respectively, Tafel curves (5 mV/s sweep rate) and Nyquist plots (100 kHz- 10mHz frequency range) were performed at room temperature. All electrodeposited specimens

were cleaned, activated by 10 vol.% HCl and immersed in the test solution for 15 minutes prior to electrochemical testing.

3. RESULTS AND DISCUSSION

3.1. Electrochemical aspects of electrodeposition

In order to investigate the electrochemical aspects of the deposition of NiW thin films, cyclic voltammograms and EIS were performed. Cyclic voltammograms were carried out with different scanning rates in order to identify the conditions for the best readability of data. The choice fell on the 50 mV/s rate for cyclic voltammetry experiments. Fig.1(a) shows the cathodic part of CV scan readings of the working electrode (Pt), drawn in NiW electroplating bath at room temperature and different pH values. In acidic medium (pH 3), the signal of hydrogen evolution reaction commencing at ≈ -0.45 V, is observed when the potential is swept negatively. With increase of bath pH (6-9), hydrogen evolving is observed to proceed at higher overpotentials and the cathodic current decreased dramatically. It is established that in a citrate electrolyte, the prevailing species depends on the solution pH. The dominant species at pH 3 are CitH_2^- and CitH_3 [20]. As the pH increases to more basic values, the citrate ion is progressively deprotonated and Cit^{3-} is the dominant species, thought to adsorb and block the electrode surface [21]. In addition, the formation of various stable complexes with metal ions, lead the reduction reactions to occur at more negative potentials. From these curves, potential values ranging from -0.9 to -1.4 V vs SCE belonging to the activation and mixed activation-diffusion control regions were selected for electrodeposition.

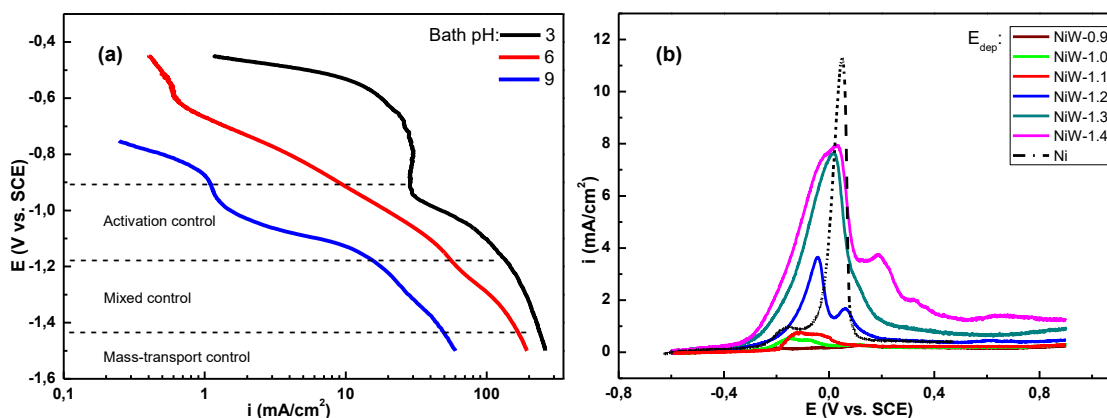


Figure 1. Cathodic polarization plots of NiW obtained in plating bath at various pH values (a) and anodic part of CVs of deposits obtained potentiostatically at pH6 and variable cathodic limit (b). Scan rates: 50 and 5 $\text{mV}\cdot\text{s}^{-1}$ respectively.

The set of electrochemical processes can be better illustrated when the cathodic limit scan is progressively moved. The potential was swept between +1.0 and -1.4 V/SCE, beginning from the open circuit potential (OCP) towards cathodic direction. Fig. 1(b) shows the anodic parts of the voltammograms. It can be clearly seen that the anodic peak of NiW film is broader compared to that of

pure nickel. With extending the cathodic limit, additional anodic peaks appeared and shifted in the positive direction, suggesting that fundamental changes occur at the surface. The presence of similar two anodic peaks in non-stirred electrolyte was reported by Obradovic and co-workers [22], according to whom only alloys with substantial W content do exhibit multiple anodic peaks, and the deposit layers contained a mixture of Ni, W, $(\text{Ni}(\text{OH})_2)$ and WO_3 .

EIS experiments were taken from the frequency of 100 kHz to 10 mHz with the sinusoidal amplitude of 10 mV, after the electrode (pure copper sheet) reaches a steady state (about 15 min). A family of Nyquist plots measured during the reduction of nickel-and tungsten species is shown in Fig. 2.

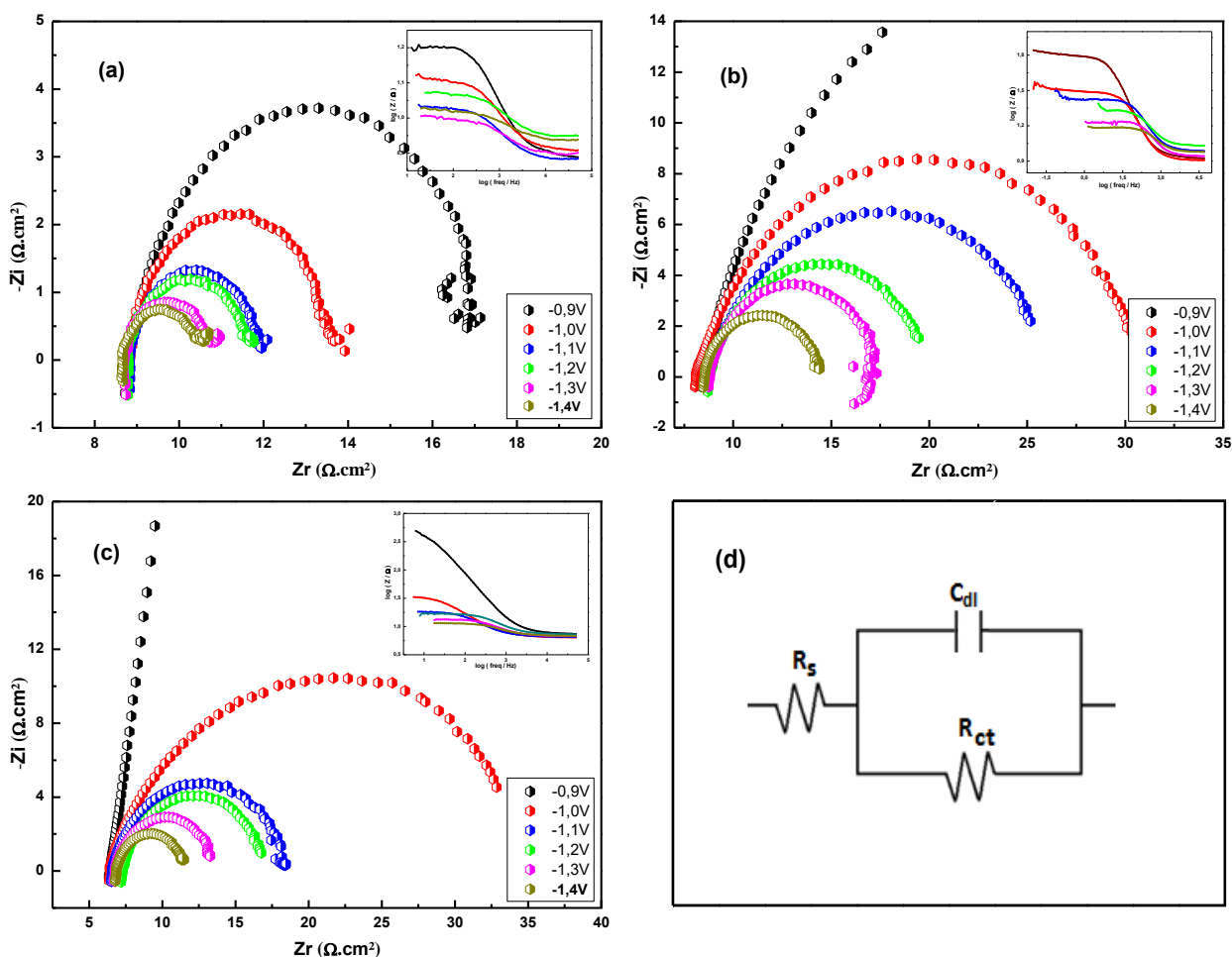


Figure 2. Nyquist plots for NiW film electroplating at different deposition potentials and at bath pH: 3(a), 6(b) and 9(c). The inserts present the corresponding Bode plots. Figure (d) shows the equivalent circuit for the high to medium - frequency impedance curves during the electrodeposition of NiW alloy.

The plots have almost the same shape for all deposits. The applied potentials at which complex-plane impedance was measured are indicated in the figure. The inserts present the corresponding Bode plots showing a single time constant and indicating that only one mechanism is

prevailing in the deposition process. Each plot is composed of a depressed semicircle resulting from the parallel combination of charge transfer resistance and capacitance, observed at high to medium-frequency region. The presence of only one main loop in the Nyquist plots indicates that the electroplating process of NiW films is under activation control [5]. The curves were fitted using the Randel's circuit [23] and the equivalent circuit is shown in Fig.2(d). At low frequencies, a very small inductive loop is also observed and particularly more pronounced in acidic electrolyte [Fig.2(a)]. The appearance of the inductive loop at low frequencies is generally ascribed to the existence of relaxation process of a single adsorbed intermediate during electrodeposition [24], such as hydrogen complex ions NiH^+ as reported by Badawy *et al.*[25]. The charge transfer resistance (R_{ct}) values were extracted from the Nyquist plots in [Fig.2(a-c)] by the intercept segment of the semicircle with the real axis. The influence of the applied cathodic potential (E_{appl}) on R_{ct} is plotted in Fig.3, where it can be seen that R_{ct} decreases with E_{appl} exponentially. The experimental data in the figure are presented as points and the continuous lines are obtained by curve fitting using the ORIGIN software. It is established that in the case of low cathodic overpotentials, the co-deposition follows a 3-D progressive nucleation/growth mechanism, while higher overpotentials favor the instantaneous nucleation [26]. For example, at pH 3.0, 6.0 and 9.0, the decrease of R_{ct} values from 9.43, 284 and 405.1 $\Omega\cdot\text{cm}^2$ at -0.9 V/ SCE to 1.93, 15.28 and 22.57 $\Omega\cdot\text{cm}^2$ at -1.4 V/SCE respectively, should indicate that the nucleation/growth process of NiW film onto the pre-formed homogeneous layer of the same compound are much easier than that onto the heterogeneous copper substrate surface.

The reaction rate for a cathodic reaction at a solid electrode-electrolyte interface under activation control such as $Ox + ne^- \rightarrow Red$ may be expressed by differentiating the Faraday's law of electrolysis, $m = I_c t / nF$ with respect to time:

$$dm / (dt = I_c / nF) \quad (1)$$

Where m (in moles), is the amount of resulting material; dm/dt represents the rate of formation of product; i , the current intensity and F , the Faraday constant. As electrochemical reactions are surface processes, it is usually convenient to relate the reaction rate to the electrode area, A [27]. The above equation may be rewritten as:

$$dm/Adt = i/nF \quad (2)$$

This represents a balance between the flux of mass and the electron flux at the electrode/electrolyte interface. On the other hand, for large and negative activation overpotentials η , the reaction rate in terms of the cathodic current density i_c , can be expressed according to the Butler-Volmer equation [28]:

$$i_c = i_0 \exp\left(-\frac{\beta nF\eta}{RT}\right) \quad (3)$$

i_0 and β being the exchange current density and the cathodic transfer coefficient assisting the reaction in the forward direction, respectively,

By combining eq (2) and eq (3), the relationship between the electrochemical reaction rate constant K of the reaction: $Ox + ne^- \rightarrow Red$ and the applied overpotential η can be established as follows:

$$K = K_0 \exp\left(-\frac{\beta nF\eta}{RT}\right) \quad (4)$$

Where K and K_0 are the rate constants for reduction at E and $E_{i=0}$, with respect to the reference electrode respectively. Therefore, the greater the applied voltage, the larger the resulting current flux, and the greater the electrochemical reaction rate constant K at the electrode/electrolyte interface. This causes the exponential decay of the charge transfer resistance R_{ct} , with increasing the applied overpotential.

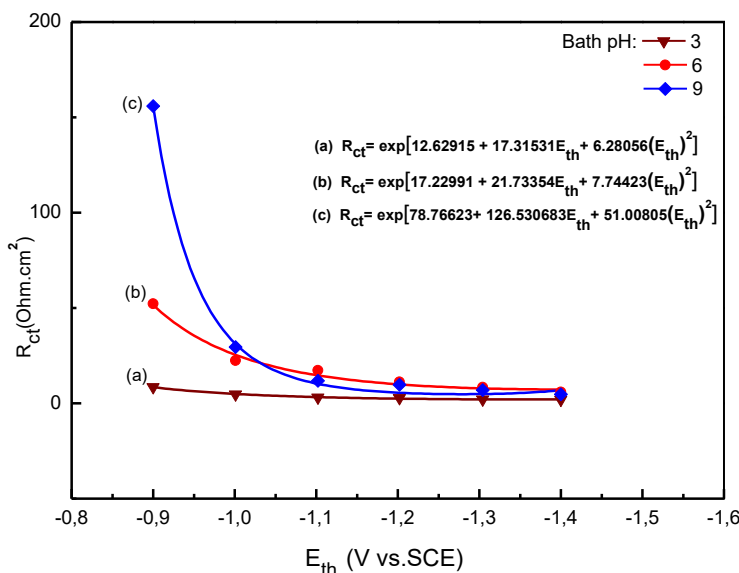


Figure 3. Experimental (symbols) and fitted (solid lines) variations of R_{ct} with bath pH and applied cathodic potential E_{appl} .

3.2. Composition and structural investigation

Energy dispersive spectroscopy (EDS) was used to measure the percentage of tungsten in the films. Table 1 provides W content of the Ni-W alloys as a function of the applied potential during the deposition. The electrodeposition was performed by applying a cathodic potential ranging from -0.9 to -1.4 V vs. SCE, in the electrolyte of a fixed pH. As seen, the content (at.%) of W in the deposit increased with a.p., until it reached a maximum of 31.67 at.% (59.22 wt.%) at -1.2 V vs. SCE, above which the W content was found to be decreased in the deposit. Similar behavior was observed by Elias *et al.* [5] for NiW alloys coated under galvanostatic regime.

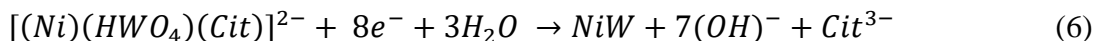
It is well established that, as a ligand, citrate forms several complex ions with nickel. In a citrate bath at low pH values ($pH \leq 3$), the solution contains mainly $NiCitH$ species in addition to free nickel ions. As the bath pH increases, the chelates are progressively deprotonated and the free nickel ions disappear [29]. At a pH ranging from 5 to 7, the predominant citrate species is the ion with three negative charges, Cit^{3-} which is assumed to form the prevailing $NiCit^-$ and $NiCit_2^{4-}$ complexes. On the other hand, according to Cruywagen *et al.* [30], in presence of citrate ions, the tungstate ion, WO_4^{2-} forms complexes in the form of $[(WO_4)_p(Cit)_qH_r]^{(2p+3q-r)-}$, in spite of the fact that both are negatively charged where, the number of protons, r , depends on the pH. In the range of pH of 2 to 4,

the predominant complex is $[(WO_4)(Cit)(H)_3]^{2-}$. The less protonated form $[(WO_4)(Cit)(H)_2]^{3-}$ is predominant at pH 6, while at pH 8.5, the prevailing complex is in the form $[(WO_4)(Cit)(H)]^{4-}$.

The deposition of NiW alloys is thought to occur via the formation of a precursor of the type $[(Ni)(HWO_4)(Cit)]^{2-}$ [31]. Nickel-citrate reacts with tungstate-citrate to form a ternary complex in the bulk of the solution or on the surface:



The reduction of this ternary precursor leads to the formation of the Ni/W alloy:



However, this complex has not been yet detected, either in solution or an adsorbed species. For low overpotentials, the NiW co-deposition may be due the firstly adsorbed and reduced Ni ions followed by adsorption of tungstate onto the nickel sites. The adsorption of tungsten ions inhibits subsequent deposition of nickel and leads to the preferential deposition of W, although it does not completely block Ni deposition. By increasing the overpotential, the tungsten content in the deposit increases until it reaches its maximum at around -1.2 V vs SCE. Going more negative than 1.2 V, results in a decrease of W amount in the deposit due to the fact that, under these conditions, the reduction of tungstate is proven to be a mass-transport controlled reaction due to the low concentration of the corresponding electroactive complex [32-33].

The variations of W content in NiW alloys with pH was also investigated by varying pH from 3 to 9 at a fixed applied potential and results are shown in Table 1. As seen, changes of the W content in the alloys are significantly correlated with the bath pH. The maximum amount of W in the deposit is obtained at pH 6; at a lower or a higher electrolyte pH, the amount of W drastically decreases. The deposition of nickel from acidic electrolyte could occur by a direct discharge of free Ni(II) ions, NiCitH species and the ternary complex formed in ammonia-free citrate baths. At pH 6, the concentration of $[(WO_4)(HCit)(H)_2]^{3-}$ electroactive complex ions in solution reaches its maximum [30], leading to an increase in the W content. Further increase of the pH up to 9 without ammonia, the deposits were of poor quality. In the presence of ammonia, a significant decrease of the tungsten content of the alloy was observed. This is in line with the views of Ernst *et al.* [34] who reported that addition of NH_3 into solutions containing citrate and ions of the iron-group metals, leads to the formation of a complex of the form of $[M(HCit)(NH_3)_3]^-$, which is reduced more easily than the citrate-complex. On the other hand, the free tungsten ion, WO_4^{2-} which is the predominant species at this pH value is deactivated and cannot participate in the reduction reactions to form Ni-W alloys.

Under these conditions, it is obvious that the relative decay of W-content in the deposit is mainly due to the formation of the ammonia-citrate complex that facilitates Ni deposition.

The effect of these two electrolysis parameters (E and pH) on the structure of NiW electrodeposits was also investigated. Figure 4 shows X-Ray diffraction patterns NiW alloys deposited at different potentials from a citrate plating bath at pH=6 and room temperature. For the sake of comparison, patterns for pure Ni and NiW alloy deposited at solution pH 9 are also inserted in the figure. Alloys obtained from acidic bath (pH3) showed similar structure to those deposited from pH6 and are not reported here. It can be seen that with increasing the overpotential (i.e. increasing W content) the cathodic overpotential yielded a broadening of the Ni(111) diffraction lines and a slight shift to lower angles, compared to that of pure nickel (JCPDS #04-0850), until overlapping with that of

the copper substrate peak (JCPDS #04-0836), indicating the formation of amorphous solid Ni(W) solution and lattice expansion due to the substitution of Ni atoms by W atoms, the atomic radius for W and Ni being 140 pm and 124 pm respectively [35]. At the same time, the intensities of (200) and (220) signals decreased markedly, which indicate a more reduced crystallinity of the deposits and supports the findings reported by other research groups [36-37]. NiW alloys deposited from alkaline solution (pH9) showed better crystallinity, probably due the lowered W composition.

The crystallite size of the deposits was calculated by the Scherrer's formula [38]:

$$d = \frac{0.9\lambda}{\beta \cos\theta}$$

Where: λ , θ and β are the X-ray wavelength of $CuK\alpha$ (1.5406 \AA), the Bragg diffraction angle and the full width at half maximum (FWHM) of fcc -Ni (111) diffraction peak. Results showed that the worked out grain size decreases from 116 nm for pure nickel to 106.32 nm and 95.58 nm for for NiW layers deposited at -1.2 and -1.4 V vs. SCE for pH6 and 113.94 nm for pH9 respectively, supporting the findings in XRD investigations.

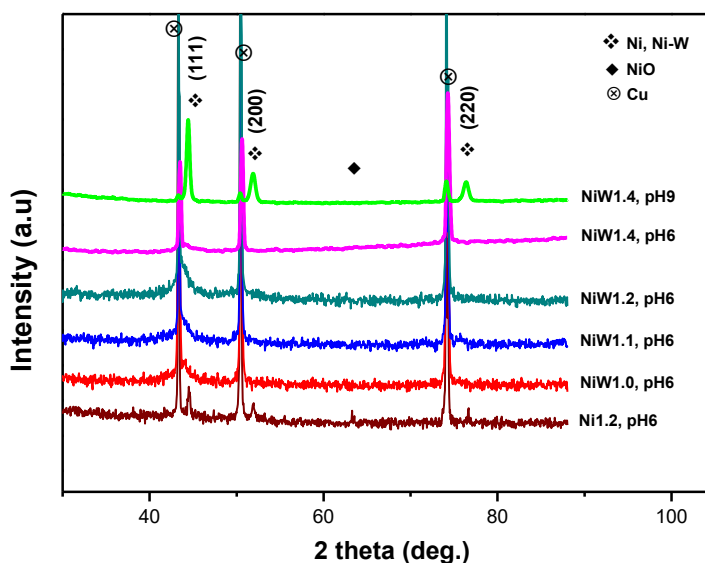


Figure 4. X-ray diffraction patterns of Ni-W alloys electrodeposited at different cathodic potentials from a citrate electrolyte at pH 6 and room temperature. For comparison, patterns of pure Ni and Ni-W alloy deposited from alkaline bath (pH=9) are also inserted.

3.3. Morphology of the deposits

The surface morphology and cross sectional images (SEM) of NiW layer electrodeposited at room temperature is shown in Fig. 5. As can be seen, SEM top-view image of deposits plated at -1.2 V vs. CSE from an electrolyte at pH 6 [Fig.5 (a)] shows clusters of spheroids sized between 0.5 to 2 μm , with circular or quasi-circular borders, which is quite different from the polygonal shape of polycrystals. This is in good agreement with the features expected in the formation of amorphous alloys [39]. Similar nodular morphology has been observed by other authors for NiW layers electroplated from baths based on ammonium, glycine and triethanolamine [37, 40]. NiW films obtained at -1.3 V

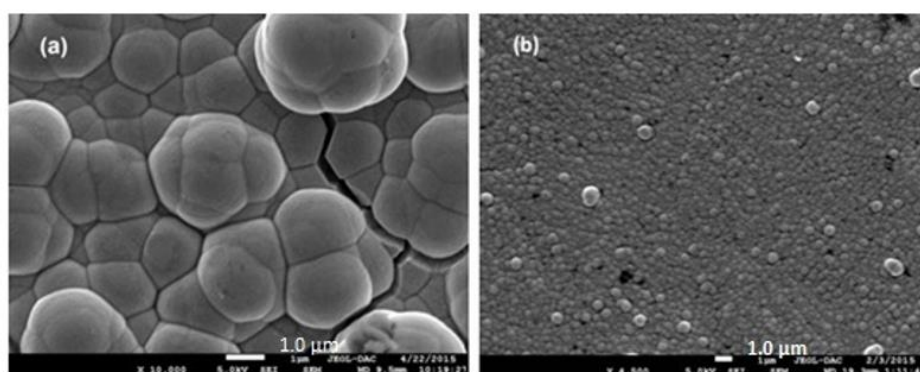
vs. SCE have globular morphology showing fewer defects [Fig.5 (b)], while deposits plated at -1.4 V vs. SCE are homogenous, dense [Fig.5 (c-d)], even though the coatings still displayed some micro-cracks, which is inherent nature of electrolytic W alloys. The coating thickness is evaluated to about $5 \mu\text{m}$. That is NiW film crystallinity increases with the decrease in W content at higher applied overpotentials. Deposits coated from acidic electrolyte ($\text{pH} = 3$) [Fig.5 (e)] contain cracks. The cracks can cross the grains indicating that they may be due to relaxation of internal tensile stress in the films. During the plating process, it is well known that hydrogen is trapped into the deposits. Subsequent release of hydrogen results in high tensile stress, which develops micro cracking in NiW structure. With increasing the plating bath pH up to 9.0, tungsten content decreases and a transition in surface morphology of the deposits from nodular to angular morphology was found [Fig.5 (f)]. This is in line with reported results on the effect of W content on the transition in texture of such deposits [41].

3. 4. Electrochemical Corrosion tests

The corrosion stability of the W-rich coatings was evaluated in 3.5 wt.% NaCl medium using potentiodynamic polarization and electrochemical impedance spectroscopy techniques.

Table 1. The composition and corrosion behaviors of Ni–W alloy electrodeposited at different bath pH and applied potentials (E_{appl}) values.

Deposit Parameters	NiW									Ni
	1.0	1.1	1.2			1.3	1.4			
$-E_{\text{dep}}(\text{V/SCE})$	1.0	1.1	1.2	1.2	1.2	1.3	1.4	1.4	1.4	1.2
pH	6	6	3	6	9	6	3	6	9	6
W (at. %)	28.66	30.98	18.47	31.67	22.37	18.46	9.27	14.11	9.03	0
$-E_{\text{corr}}(\text{mV/SCE})$	701.2	683.9	456.7	572.1	538.2	654.5	665.8	746.0	573.6	644.3
$j_{\text{corr}}(10^2 \cdot \text{mA/cm}^2)$	0.85	1.19	5.63	0.63	0.80	0.76	06.20	02.91	0.87	1.34
$\text{CR} \times 10^{-2} (\mu\text{m} \cdot \text{y}^{-1})$	99.03	138.7	657.9	73.95	93.37	89.11	725.4	340.1	102	156.4



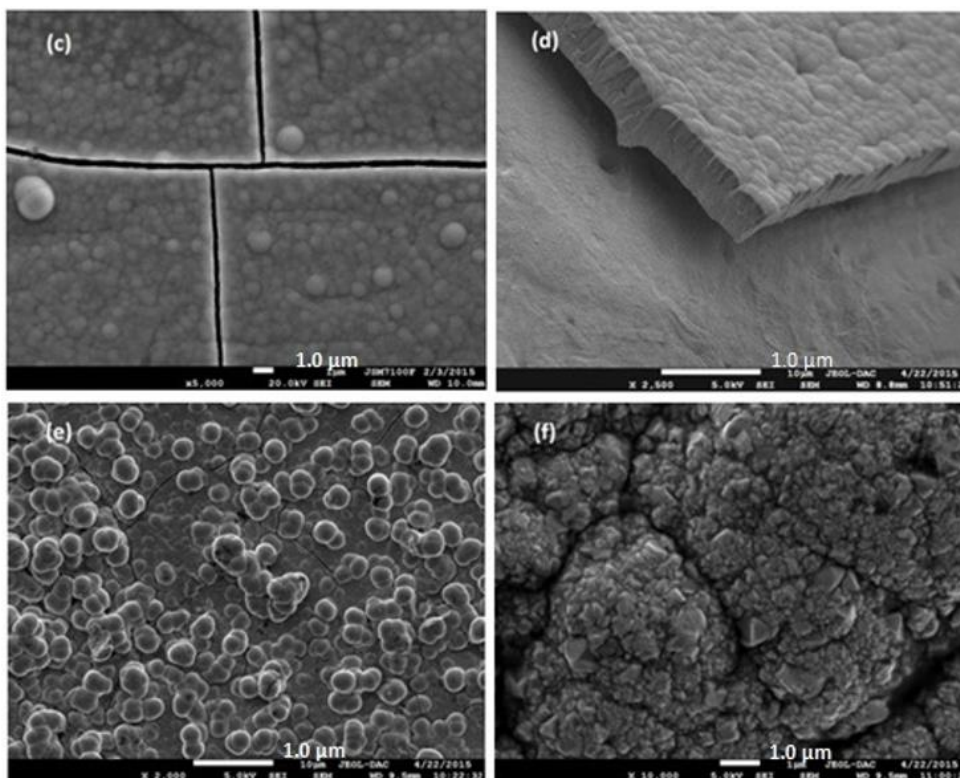


Figure 5. FESEM images of NiW samples deposited at pH 6 and E(V vs. SCE): -1.2 V (a), -1.3 (b), -1.4 (c-d). Alloys obtained at -1.4 V and pH: 3(e) and 9 (f).

Tafel polarization curves for NiW alloys plated at $\text{pH} \approx 6$ and variable applied potentials are shown in Fig. 6. For comparison with the behaviour of the deposited alloys, the curve of pure electrodeposited Ni was recorded. The corrosion data for all alloys, reported in Table 1 testify that corrosion rate of NiW deposits decreased with increasing applied cathodic potential up to ≈ -1.2 V/CSE, and then increased.

Therefore, it can be concluded that the Ni-W alloy, deposited at -1.2 V/ SCE with the highest W content (32 at.%) was found to be more corrosion resistant compared to all alloys deposited from the same bath. Furthermore, the electrochemical impedance results showed the same trend as polarization. The Nyquist response of NiW alloy deposited at -1.2 V/SCE is of maximum radius compared to those obtained at other overpotentials, indicating that it offers better electrochemical behavior in 3.5 wt.% NaCl, compared to the other coatings. The corrosion stability of such an alloy may be a result of increased surface area due to microcracks and the formation of a layer of mixed nickel-tungsten oxides (NiO, NiOOH and WO_3) as reported by Quiroga Arganaraz *et al.* [42] and Vasko [43], who assumed the formation of an adsorbed nickel hydroxide layer on the electrode, which reacts with tungstate ions to form a mixed oxide. Moreover, Obradovic *et al.* [22], reported that stable and protective surface oxide layer, a mixture of Ni, W, $\text{Ni}(\text{OH})_2$ and WO_3 , is obtained only for alloys with high W- content. As the deposition potential is increased further, the W content of the alloy decreases; the amounts of Ni and W oxides decrease as well due to their rapid reduction to the metal form by atomic hydrogen adsorbed on the electrode surface leading to less protected coating in

corrosive environment. Moreover, Obradovic and co-workers [33] suggested that Ni(I) intermediate species in the deposition of Ni could have substantial reducing effect of the W-oxides formed at the electrode-electrolyte interface.

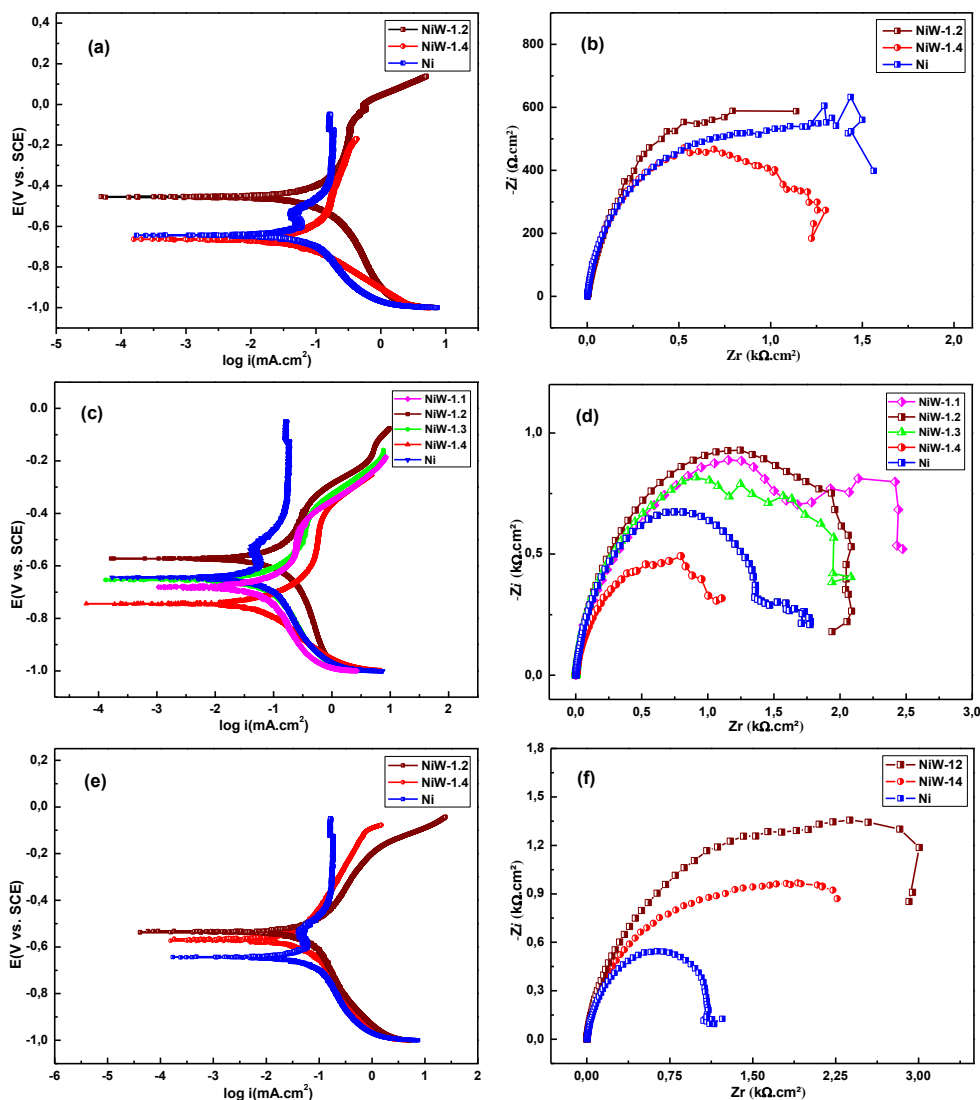


Figure 6. Potentiodynamic polarization behavior and Nyquist plots for Ni and NiW deposits obtained at different applied potentials (as indicated in the figures) and bath pH: 3 (a-b), 6(c-d) and 9(e-f). Scan of 5 mV/s in 3.5 wt.% NaCl solution.

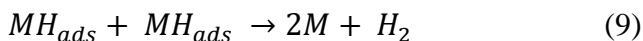
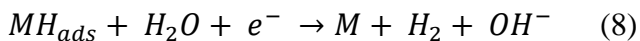
3. 5. Electrocatalytic properties

The electrocatalytic activity of NiW coatings for hydrogen production was investigated by means of linear polarization and the kinetic parameters for the HER were derived from Tafel equation [44]:

$$\eta = a + b \log j$$

where η (V), a (V), b (V.dec⁻¹) and j (A.cm²) represent the applied overpotential, the intercept, the Tafel slope and the resulting current density respectively.

The general model usually proposed for the hydrogen evolution reaction (HER) mechanism in alkaline media [45] involves the formation and adsorption of hydrogen ad-atoms at the electrode surface (MH_{ads}), known as the Volmer reaction (Eq.7) followed by an electrochemical desorption, Heyrovsky step (Eq.8) or by a chemical recombination step, known as Tafel reaction (Eq.9):



Depending on which of these reactions is the rate determining step (RDS), the resulting Tafel curves should yield, at 25 °C, a slope of 120, 40 or 30 mV.dec⁻¹ for Volmer, Heyrovsky or Tafel reaction respectively [45].

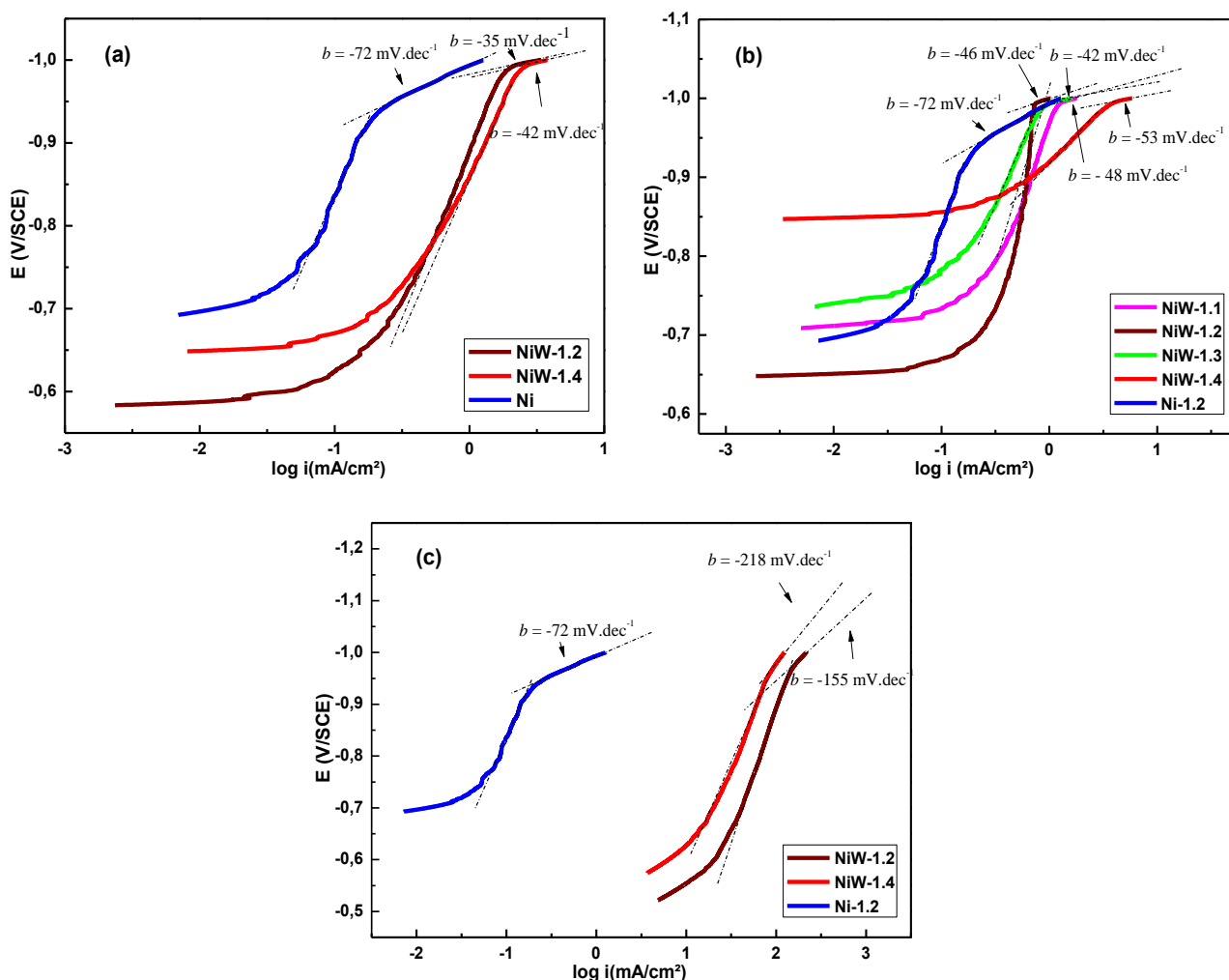


Figure 7. Tafel plots of Ni-W alloy coatings in 30 wt.% KOH as function of bath pH values: 3(a), 6(b) and 9(c) and various deposition potentials (as indicated in the figures).

Figure 7 shows the Tafel plots recorded in 30 wt.% KOH on Ni-W catalysts electrodeposited at various potentials and bath pHs, and Table 2 collects the corresponding kinetic parameters. From these data, it can be clearly seen that Ni-W alloys obtained at high overpotentials (i.e $E_{\text{appl}} \sim -1.4$ V vs. SCE) yield the highest HER catalytic activity, compared to all the remaining cathodes, as a result of possible synergism between Ni and W, according to Brewer-Engel theory [46]. The Tafel slope, b , for high overpotential region is in the 35-55 mV.dec^{-1} range, indicating that on NiW alloys, hydrogen evolution reaction follows the Heyrovsky mechanism, excepted for pH9 where the derived slope is over 120 mV.dec^{-1} , corresponding to the Volmer-Heyrovsky step as RDS. On the other hand, the W-richest alloy (NiW-1.2, 31.67 at.% W) seems to be the worst HER electrocatalyst (lowest exchange current density- j_0) even though it's slope is of only 46 mV.dec^{-1} , most probably due to the existence of W oxides on the electrode surface [4].

Table 2. Kinetic parameters for the HER obtained from the polarization curves of Ni-W coatings recorded in 30 wt.% KOH solution.

Deposit Parameters	NiW								Ni
	1.1	1.2			1.3	1.4			1.2
- E_{dep} (V)	1.1	3	6	9	6	3	6	9	6
pH	6	3	6	9	6	3	6	9	6
W (at. %)	30.98	18.47	31.67	22.37	18.46	9.27	14.11	9.03	0
- E_{eq} (mV/SCE)	-708.9	583.5	-648	-521.7	-736	648.5	-847.8	-574.2	692.5
$j_0(10^{-2}.\text{mA.cm}^2)$	13.19	12.67	0.02	0.521	9.89	18.83	30.07	0.134	7.19
$b_c(\text{mV.dec}^{-1})$	48	35	46	155	42	42	53	218	72

4. CONCLUSION

In this study, the formation of amorphous W-rich NiW alloys by electrodeposition under potentiostatic conditions from ammonia-free citrate electrolyte is investigated. The results obtained from cyclic voltammetry, potentiodynamic polarization and electrochemical impedance match well one to another. The use of strong acidic solutions accentuate the generation of internal stresses resulting in the formation of microcracks. Alloys coated from alkaline electrolyte without ammonia led to non-uniform and less adherent to the substrate deposits. High corrosion resistance of W-rich NiW alloys plated under activation control at -1.2 V/SCE (having about 32 at.% W) from slightly acidic bath (pH6), superior to those of pure Ni and low-W content deposits, was attributed the presence of stable and protective surface oxide layer. The best HER activity was observed for alloys deposited under mixed activation-diffusion regime at -1.4 V/SCE (having about 14 at.% W) following the

Volmer-Heyrovsky mechanism and ascribed to both increased surface area of active centers due to microcracks and electrocatalytic synergism of Ni and W for the hydrogen evolution reaction.

ACKNOWLEDGEMENTS

The authors gratefully acknowledge the financial support provided by the Algerian Directorate General for Scientific Research and Technological Development (PNR Project no.10/u19/4191). We would like also to thank Dr A. Boukeroui (Bejaia University, Algeria) for helping in the X-ray analysis.

References

1. M. F. Horddeski, *Alternative Fuels - The Future of Hydrogen*, Fairmont Press, Lilburn (2007).
2. K. Liu, C. Song and V. Subramani, *Hydrogen and Syngas Production and Purification Technologies*, Wiley & Sons, New Jersey (2010).
3. J. K. Nørskov, T. Bligaard, A. Logadottir, J. R. Kitchin, J. G. Chen, S. Pandalov and U. Stimming, *Journal of the Electrochemical Society*, 152(3) (2005) J23.
4. E. Navarro-Flores, Z. Chong and S. Omanovic, *Journal of Molecular Catalysis A: Chem.*, 226 (2005) 179.
5. L. Elias, K. Scott and AC. Hegde, *Journal of Materials Engineering and Performance*, 24(11) (2015) 4182.
6. S. Lee, M. Choi, S. Park, H. Jung and B. Yoo, *Electrochimica Acta*, 153 (2015) 225.
7. K. R. Sriraman, S. G. S. Raman and S. K. Seshadri, *Materials Science and Engineering A*, 418 (2006) 303.
8. A. Brenner, *Electrodeposition of Alloys: Principles and Practice*, Academic Press, New York (1963).
9. M. Wang, Z. Wang and Z. Guo, *Materials Chemistry and Physics*, 148 (2014) 245.
10. M. P. Marceta-Kaninski, D. P. Saponjic, I. M. Perovic, A. D. Maksic and V. M. Nikolic, *Applied Catalysis A: General*, 405 (2011) 29.
11. O. Younes, L. Zhu, Y. Rosenberg, Y. Shacham-Diamand and E. Gileadi, *Langmuir*, 17 (2001) 8270.
12. O. Younes and E. Gileadi, *Electrochem. Solid State Lett.*, 3 (2000) 543.
13. S. H. Hong, S. H. Ahn, J. Choi, J. Y. Kim, H. Y. Kim, H. J. Kim, J. H. Jang, H. Kim and S. K. Kim, *Applied Surface Science*, 349 (2015) 629.
14. C. LI, X. Li, Z. Wang and H. Guo, *Trans. Nonferrous Met. Soc. Ch.*, 17 (2007) 1300.
15. M. Pushpavanam and K. Balakrishnan, *J. Appl. Electrochemistry*, 26 (1996) 1065.
16. M. Ishikawa, H. Enomoto, M. Matsuoka and C. Iwakura, *Electrochimica Acta*, 40 (1995) 1663.
17. A. R. Despic, V. D. Jovic and S. Spaic, *J. Electrochem. Soc.*, 136 (1989) 1651.
18. N. Eliaz and E. Gileadi, *Modern aspects of electrochemistry*, Springer, New York (2008).
19. M. Schlesinger and M. Paunovic, *Modern Electroplating*, Wiley & Sons, New Jersey (2010).
20. S. Rode, C. Henninot, V. Cecile and M. Matlosz, *Journal of Electrochemical Society*, 151 (2004) C405.
21. E. Chassaing, K. V. Quang and R. Wiart, *J. Appl. Electrochemistry*, 16 (1986) 591.
22. M. Obradovic, J. Stevanovic, A. Despic, R. Stevanovic and J. Stoch, *J. Serb. Chem. Soc.*, 66 (2001) 899.
23. J. R. Macdonald (Ed.), *Impedance Spectroscopy*, Wiley & Sons, New York (1987).
24. V.F. Lvovich, *Impedance spectroscopy: Applications to electrochemical and dielectric phenomena*, Wiley & Sons, New Jersey (2012).
25. W. A. Badawy, F. M. Al-Kharafi and J. R. Al-Ajmi, *Journal of Applied Electrochemistry*, 30 (2000) 693.
26. J. F. Li, Z. Zhang, J. Y. Yin, G. H. Yu, C. Cai and J. Q. Zhang, *Trans. Nonferrous Met. Soc. China*, 16 (2006) 659.

27. D. Santos, C. Sequeira and J. Figueiredo, *Quim. Nova*, 36 (2013) 1176.
28. E. Santos and W. Schmickler, *Catalysis in Electrochemistry: From fundamentals to strategies for fuel cell development*, Wiley & Sons, New Jersey (2011).
29. S. Rode, C. Henninot and M. Matlosz, *Journal of the Electrochem. Society*, 152 (4) (2005) C248.
30. J. J. Cruywagen, L. Kruger and E. A. Rohwer, *J. Chem. Soc. Dalton Trans.*, (1991) 1727.
31. N. Eliaz, T. M. Sridhar and E. Gileadi, *Electrochimica Acta*, 50 (2005) 2893.
32. S. Kabi, K. Raeissi and A. Saatchi, *J Appl Electrochem*, 39 (2009) 1279.
33. M. D. Obradovic, R. M. Stevanovic and A. R. Despic, *Journal of Electroanalytical Chemistry*, 552 (2003) 185.
34. D. W. Ernst, R. F. Amlie and M. L. Holt, *J. Electrochem. Soc.*, 102 (1955) 461.
35. B. K. Vainshtein, V. M. Fridkin and V. L. Indenbom, *Modern Crystallography: Structure of Crystals*, Springer, Berlin (2000).
36. A. Królikowski, E. Płońska, A. Ostrowski, M. Donten and Z. Stojek, *J Solid State Electrochem.*, 13 (2009) 263.
37. I. Mizushima, P. T. Tang, H. N. Hansen and M. A. J. Somers, *Electrochimica Acta*, 51 (2005) 888.
38. B. D. Cullity and S. R. Stock, *Elements of X-ray diffraction*, Prentice Hall, New Jersey (2001).
39. F. E. Lubovsky, *Amorphous Metallic Alloys*, Butherworths Publishers, Ontario (1983).
40. Y. Wu, D. Y. Chang, S. C. Kwon, D. Kim, *Plat. Surf. Finishing*, 2 (2003) 46.
41. S. Ruan and C. A. Schuh, *Scripta Materiala*, 59 (2008) 1218.
42. M. P. Quiroga Argañaraz, S. B. Ribotta, M. E. Folquer, G. Benítez, A. Rubert, L. M. Gassa, M. E. Vela and R. C. Salvarezza, *J. Solid State Electrochemistry*, 17 (2013) 307.
43. A. T. Vasko, *Encyclopedia of Electrochemistry of the Elements*, Marcel Dekker, New York (1986).
44. T. J. Kemp, *Instrumental Methods in Electrochemistry*, Ellis Horwood Ltd, Chichester (1985).
45. N. Tsyntaru, H. Cesiulis, M. Donten, J. Sort, E. Pellicer and E. J. Podlaha-Murphy, *Surface Engineering and Applied Electrochemistry*, 48 (2012) 491.
46. M. M. Jaksic, *Electrochimica Acta*, 45 (2000) 4085.